

- 477–481 (1998).
7. Röseler, A. & Korte, E. H. Surface enhanced infrared absorption observed with attenuated total reflection (ATR-SEIRA): modeling the optical response. *Fresenius J. Anal. Chem.* **362**, 51–57 (1998).
 8. Lewis, A., Isaacson, M., Haroutunian, A. & Muray, A. Development of a 500 Å spatial resolution light microscope. *Ultramicroscopy* **13**, 227–232 (1984).
 9. Pohl, D. W., Denk, W. & Lanz, M. Optical stethoscopy: Image recording with resolution $\lambda/20$. *Appl. Phys. Lett.* **44**, 651–653 (1984).
 10. Piednoir, A., Licoppe, C. & Creuzet, F. Imaging and local infrared-spectroscopy with a near-field optical microscope. *Opt. Commun.* **129**, 414–422 (1996).
 11. Knoll, B., Keilmann, F., Kramer, A. & Guckenberger, R. Contrast of microwave near-field microscopy. *Appl. Phys. Lett.* **70**, 2667–2669 (1997).
 12. Bohren, C. F. & Huffman, D. R. Absorption and scattering of light by small particles. (Wiley & Sons, New York, 1983).
 13. Völcker, M., Krieger, W. & Walther, H. Detection of local conductivity by laser-frequency mixing in a scanning force microscope. *J. Appl. Phys.* **74**, 5426–5431 (1993).
 14. Otto, A., Mrozek, I., Grabbhorn, H. & Akemann, W. Surface-enhanced Raman scattering. *J. Phys.: Condens. Matter* **4**, 1143–1212 (1992).

Acknowledgements. We thank H. Sturm for supplying samples and A. Röseler for supplying spectral data. Discussions with R. Guckenberger, A. Kramer, and D.v.d. Weide are acknowledged.

Correspondence and requests for materials should be addressed to F.K. (e-mail: keilmann@biochem.mpg.de)

Radon emanation and electric potential variations associated with transient deformation near reservoir lakes

M. Trique*, P. Richon†, F. Perrier*, J. P. Avouac* & J. C. Sabroux†

* Laboratoire de Détection et de Géophysique, DASE, Commissariat à l’Energie Atomique, BP 12, F-91680 Bruyères-le-Châtel, France

† Institut de Protection et de Sécurité Nucléaire, 60-68, BP 6, F-92265 Fontenay aux Roses, France

Two of the most often cited earthquake precursors are radon emanation and electric potential variations^{1–6}, but these few reported examples have generally been deemed questionable^{7–11}. If a mechanism relating crustal deformation to radon emanation or electrical signals does indeed exist, it is thought to involve fluids^{12–19}. Some preliminary insight has been gained into these processes from the study of natural systems under controlled mechanical and hydrological conditions²⁰. Here we report electric potential variations, radon emanation and deformation measurements recorded since 1995 in the French Alps in the vicinity of two artificial lakes which have strong seasonal variations in water level of more than 50 metres. We observe that electric potential variations and radon emanations are repeatedly associated with transient deformation events induced by variations in lake levels. These events are characterized by a change in ground tilt which deviates from the expected elastic response, and are associated with periods of accelerating strain, which suggests that accelerated loading can enhance fluid transport properties. Qualitatively, this behaviour can be accounted for by a model in which straining induces fluid overpressure and dynamic flow in cracks. These observations may shed light on the sensitivity of rock transport properties to deformation.

The site that we studied is located in the French Alps, at the geological contact between the Belledonne crystalline basement to the west, and highly tectonized Permo-Triassic sedimentary units to the east (Fig. 1). The levels of the lakes vary on a yearly cycle by ~70 m for the Roselend lake and 50 m for Gittaz lake (see Supplementary Information). A dead-end tunnel located 600 m northeast of the Roselend dam (Fig. 1) is equipped with two long-period seismometers (to measure the tilts in the north–south and east–west directions), one microbarograph and three radon detectors. An array of electrodes, composed of 14 measurement points, and a

meteorological station were set across the Sur-Frètes ridge which separates the two lakes (Fig. 1).

The experiment has been running since November 1995. The radon activity and the north–south tilt observed in the tunnel, the potential difference between the RH and EO points (see Fig. 1) and the Roselend lake level are shown as a function of time in Fig. 2. The radon activity in the inner room in the tunnel (see Methods) is characterized by a low background level of 650 Bq m^{-3} , and by a number of bursts with amplitudes ranging from 2,000 to over $18,000 \text{ Bq m}^{-3}$ and durations of one to nine weeks. The radon bursts with amplitudes greater than $4,000 \text{ Bq m}^{-3}$ (labelled 2, 3, 4, 6, 8, 10, 11 and 13 in Fig. 2) are observed to correlate systematically with decreases of the RH-EO potential difference.

The electric potential variations are occurring between four days before and one day after the radon bursts. Their amplitudes range from –6 to –20 mV for time durations varying between 5 and 33 d. They do not scale in magnitude and duration time with the radon bursts. As these potential variations are not observed on the other dipoles connected to the point EO, they must originate at the point RH. Given that the observed transient electric potential variations

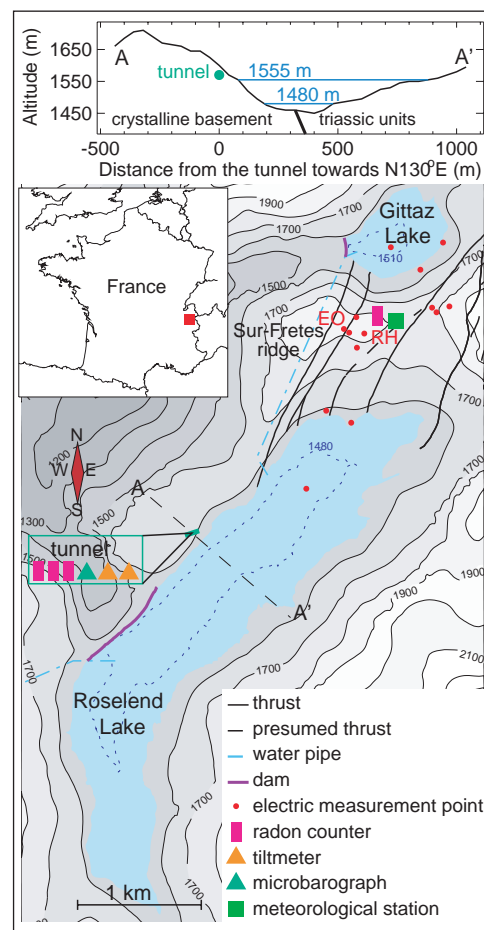


Figure 1 Layout of the Sur-Frètes experiment. The general location of the experiment is indicated by the red square in the inset to the lower figure; in the lower figure, the blue dashed curve in each lake shows the extents of the lakes at their lowest level. The topographic profile along the segment A–A' is represented in the top figure. The Roselend lake has a capacity of $187 \times 10^6 \text{ m}^3$ of water. The smaller Gittaz lake has a capacity of $13 \times 10^6 \text{ m}^3$ and communicates with the Roselend lake through an underground water pipe (blue dashed curve). The lakes are enclosed by two dams set against the crystalline rocks (purple). The lake level cycle is strongly correlated to the yearly meteorological cycle only during the snow melting phase in spring and summer. The lakes are emptied according to the needs of electric power production by a pipe (blue dashed curve) linking the Roselend lake to a power station located 15 km west.

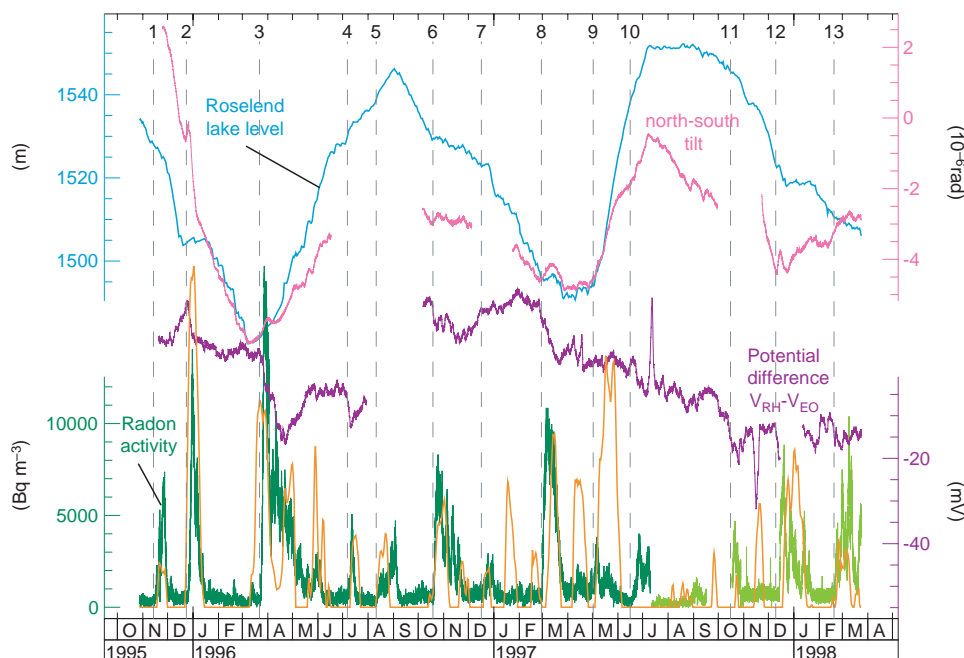


Figure 2 Temporal variations of Roselend lake level (blue), north-south tilt (red), electric potential (purple), and radon activity (green). The interruption in the series are due to storms and work on the power line. The radon activity was measured in the inner room (see Methods) from November 1995 to July 1997 (dark green), and in the corridor from July 1997 to April 1998 (light green). The north-south tilt and

electric potential data segments are arbitrarily shifted from each other. The electrical data are low-pass-filtered to remove periods <2 d, and their average value is arbitrary. The orange curve is the positive part of the discrete second derivative applied on the lake level data and expressed in arbitrary units. The lake-level data are provided by Electricité De France.

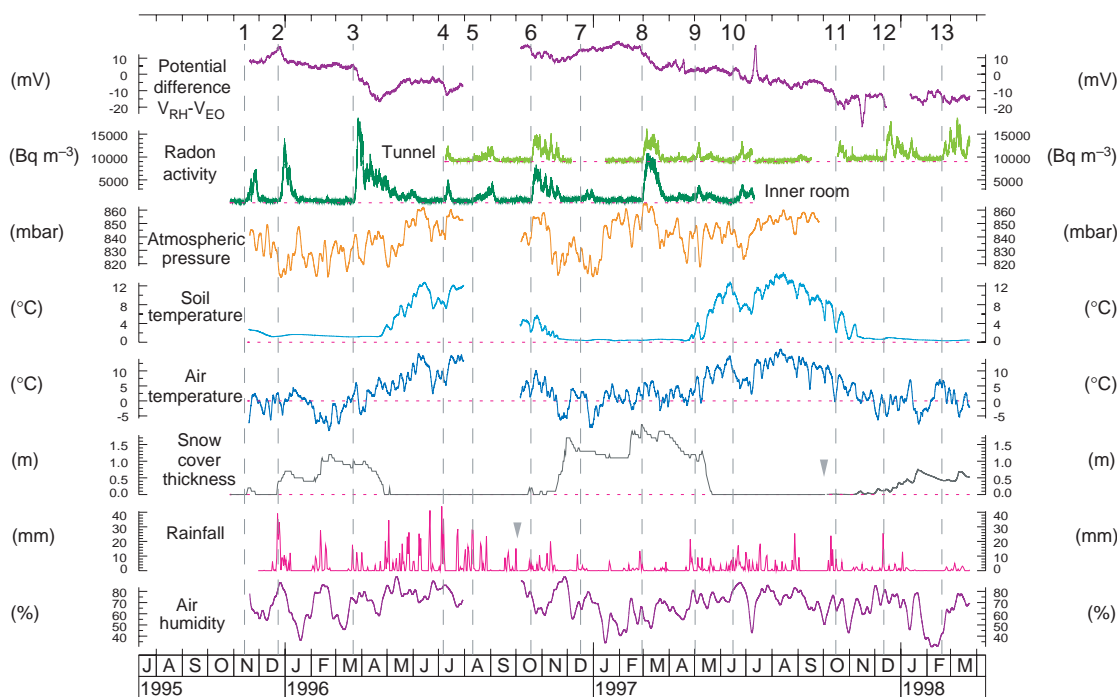


Figure 3 Potential difference of dipole RH-EO, radon activity measurements and meteorological parameters as a function of time. The meteorological parameters are recorded with a sampling interval of 5 min. The electric potential, soil temperature, atmospheric pressure, air humidity, and air temperature data are low-pass-filtered to remove the periods <2 d. The dark green curve corresponds to the autonomous radon probe located in the inner room of the tunnel, whereas the light green curve corresponds to one of the two radon probes located in the

tunnel. The grey reversed triangles indicate when the data were first acquired by the local meteorological devices. From November 1995 to October 1997, the snow height data, provided by Electricité De France, were recorded by a snowmeter located 2 km away and 150 m higher from the Sur-Frètes ridge. From October 1995 to October 1996, the rainfall data given by Météo France were acquired at Luce station located 6 km away and 800 m below the site.

do not present any pattern similar to the soil temperature data, we can exclude an electrode response to soil temperature gradients or soil humidity changes²¹. Transient electric potential variations can also be generated by the shallow water circulation²¹ systematically induced by rainfall or snow melting. A direct systematic and trivial physical relation between the rain or snow melting events and the observed electric potential variations (see Methods and Supplementary Information), and more generally with any meteorological parameters, can be excluded (Fig. 3). Also, the radon bursts are not instrumental artefacts: they are recorded by independent sensors in the tunnel (Fig. 3). The radon bursts observed in the tunnel have no systematic correlation with any local meteorological parameters (Fig. 3) which could influence the radon activity in the air of the tunnel. In particular, neither the “pumping” effect²² due to decreasing barometric pressure, nor thermal circulation through the temperature gradient between the outside and the inside of the tunnel, can explain the bursts. Other effects, such as air humidity and high-speed winds, are known to affect radon emanation²², but these can be excluded in our case; we can also exclude the blocking of the tunnel entrance by snow (Fig. 3). Rainfall, snowfall and snow melting could also affect the radon activity in the tunnel because such processes could modify the water saturation around it: but because no systematic relation appears between the signals (see Methods and Supplementary Information), this hypothesis is excluded (Fig. 3). The radon probe located on the Sur-Frères ridge did not record any similar radon bursts. The radon bursts measured in the tunnel are therefore not caused by meteorological effects.

Because the radon level in the tunnel is controlled by the radon emanation and the transport paths of the rock matrix, the variations of the radon level measured in the tunnel could be due to changes in the radon transport properties. The emanation of the rock matrix has been measured in the laboratory for dry gneiss samples, and amounts to $8.3 \text{ atoms m}^{-2} \text{ s}^{-1}$. The background radon level is therefore consistent with radon drained at the tunnel walls from a 4-cm-thick zone of saturated rocks. The radon bursts would imply either a transient change of rock saturation, from saturated to dry, or an increase of the rock volume from which the radon is drained. In the latter case, an increase of the volume of drained zone by a factor of ~ 100 is necessary to account for the radon peak levels.

The radon bursts correlate with positive-slope kinks in the plot of lake level against time (Fig. 2). We treat these kinks as follows: from the lake-level data series $h(t)$, a discrete second derivative function is built as $f(i) = h(i) - 2h(i - T) + h(i - 2T)$, where T is some fixed time delay. For a time delay of $T = 14 \text{ d}$, which was found to be most appropriate, and keeping only positive values of $f(t)$, the variations of $f(t)$ reproduce well the observed radon bursts (Fig. 2). Indeed, given a time delay between the signals ranging between -10 and 10 days, 63% of the positive variations of $f(t)$ (out of 16 events) correlate to the radon bursts (see Supplementary Information). The score is only 27% on average if the radon bursts are redistributed randomly. The proportion of the positive variations of $f(t)$ which could be related to the transient electrical variations, assuming the same time delay, amounts to 53% out of 15 events. A lesser value (30% with the same time delay) is obtained for a random time series of electrical variations. Thus, the electric and radon signals both tend to be produced by a mechanical effect, namely the accelerated straining of the medium.

This is further supported by the tilt-meter data. The tilt-meter recorded a yearly variation which amounts to several microradians and which is linearly correlated to the lake level (Fig. 2). The measured linear factor of $\sim 0.10 \mu\text{rad m}^{-1}$ is compatible with the elastic deformation due to the lake loading. Indeed, using the values of the Lamé parameters deduced from seismic sounding²³, the expected north–south tilt per metre of water amounts to $0.090 \mu\text{rad m}^{-1}$, in agreement with the observed value. The tilt-meter response is thus observed to depart from the average elastic response during the radon and electric potential anomalies. This can be clearly seen in Fig. 4, where expanded-scale views around two radon bursts (events 3 and 8) are presented. The tilt response is proportional to the lake level for constant loading velocity, but during the radon burst and coeval with the change in the potential difference, a response amplified by a factor of 3 to 5 is observed on the north–south tilt compared with the lake level.

In principle, transient tilt deformations could be generated by meteorological events; for example, by the cracks filling with water supplied by the rainfall or snow melting. However, such an artefact would appear systematically, and would also be observed with a larger amplitude at the snow-melting time. In addition, there would be no relationship between the time structure of the anomaly (basically dominated by the crack permeability) and the time structure of the lake level. We therefore consider that the tilt anomalies are not a meteorological artefact but are rather a consequence of a different mechanical response.

The time delay of 14 d required for the discrete second derivative to match the observed radon bursts (Fig. 2) suggests that the pore water may play a role. Indeed, according to the permeability (10^{-16} m^2) measured *in situ*²³, the diffusion time for a lake-level change to affect the tunnel is estimated²⁴ to range from 1 to 30 d. The different mechanical response observed for perturbations with a timescale smaller than 14 d suggests that the response then occurs in the undrained mode. However, the difference in the mechanical response between the drained and undrained conditions can at most amount to 30% (ref. 24). The observed amplification (of a factor 4 on average) must then result from another mechanism.

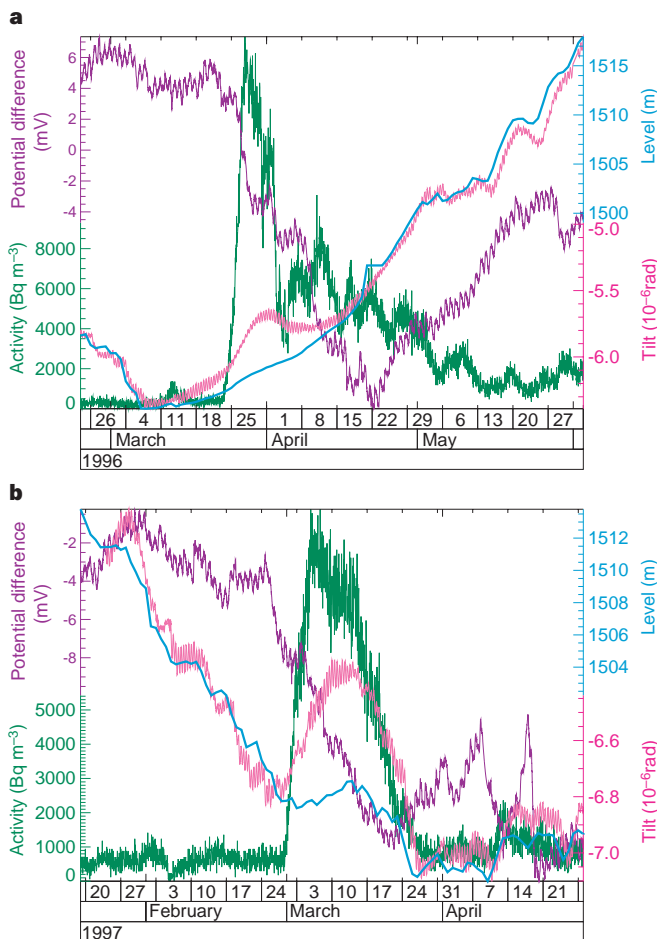


Figure 4 Roselend lake level (blue), north–south tilt (red), radon activity (green) and electric potential $V_{RH}-V_{EO}$ (purple). Data are shown for the time interval encompassing events 3 (a) and 8 (b).

The observed response may be expected from the following model. We consider a medium consisting of a low-permeability matrix with fluid-filled cracks. This model is analogous to that used to calculate the groundwater outflow in response to coseismic deformation¹⁵. If a strain rate de/dt is applied to the medium (compressive strain is considered as positive), the variation of pore volume of the cracks induces a dynamic equilibrium, in which the pore-pressure variation is balanced by the fluid flow out of the rock matrix. A first-order approximation of the pore pressure p leads to the following relationship: $p = (\eta L^2 r/k)(de/dt)$, where η is the fluid viscosity, L the characteristic length along percolation paths, k the permeability of the medium, and r the aspect ratio of the cracks. This relationship implies a pore-pressure increase (in response to accelerated lake loading) that could reach 0.1 to 1 bar, assuming a typical percolation length scale of 1 to 10 m, a permeability of crystalline rocks²³ of 10^{-16} m^2 , an aspect ratio of 10³ for the cracks, and a strain rate of 10^{-7} d^{-1} . Such overpressures may be sufficient to produce local microfracturing, and hence an increase of transport properties or the exposure of new fracture surfaces. The rapid transport to the tunnel atmosphere of the previously trapped radon gas could then account for the observed radon bursts.

The observed electric potential variations could also be produced through the electrokinetic effect by a similar enhancement of the rock transmissivity. The magnitude of the pore pressure of the fluids involved in the electrical effects can be estimated from the data of this experiment²⁵. Indeed, the variations of the potential of one point of the electrical array are linearly correlated to the Roselend lake level, with a correlation of 20 mV per 0.1 MPa (ref. 25). Using this value, the potential variations (of the order of 10 mV) observed on the RH-EO dipole could result from the connection of two systems with a 0.5-bar pore-pressure difference. This order of magnitude could be expected in the presence of an aquifer with a piezometric level higher than the mean level in the surrounding medium. Indeed, such a perched aquifer could be related to a 60-m-thick low-resistivity zone below point RH observed in a very-low-frequency electromagnetic survey performed on the Sur-Frètes ridge in July 1995 (S. Hautot and P. Tarits, personal communication).

The present experiment is not the first observation of an anelastic response to small changes in loading rate in a natural system. For example, induced seismicity near the Nurek reservoir, Tadjikistan²⁶, and the Koyna reservoir, India²⁷, appears to be controlled by the rate of change in the water level. Moreover, transient permeability enhancements have also been proposed to explain the occurrence of hydrothermal precursors to large earthquakes in northern California²⁸ and changes in hydrology occurring after large earthquakes²⁹. The physical processes involved in the signals recorded at the Sur-Frètes site may provide the basic understanding of the transport properties of kilometre-sized systems subject to stress variations: they may also be of interest for the monitoring of ground water or of waste-disposal sites. Although the applicability of our observations at the scale of active tectonic areas needs to be carefully considered, they provide an analogue to earthquake precursors, with the advantage that the mechanical forcing is known, as are the main characteristics of the medium. □

Methods

Tunnel characteristics. The nearly horizontal tunnel, drilled in gneiss, is 142 m long with a 2 m diameter, and contains an inner room of $4 \times 5 \times 2 \text{ m}$, located 60 m from the entrance and 40 m below the surface. This inner room is separated from the corridor by a metal door and the tunnel is closed by a second metal door. The inner room is not significantly ventilated, as the pressure difference between the inner room and outside has been measured to be $< 1 \text{ Pa}$. The radon background level recorded in the inner room does not show the typical seasonal variation due to air exchange driven by temperature difference between the inside and the outside, as is generally observed in caves²², attesting

again to a poor ventilation of the inner room. The tunnel closing was reinforced in October 1997 by two air-tight plastic doors to further reduce ventilation. The radon background level recorded in the tunnel rose from 250 to 650 Bq m^{-3} , as measured in the inner room, suggesting an enhancement of the air confinement in the tunnel. The air relative humidity in the tunnel is close to 100%. The temperature is stable at $6.6 \pm 0.2 \text{ }^\circ\text{C}$ over the whole year.

Tilt measurements. The tiltmeters have a resolution of 20×10^{-9} rad. They have a pressure sensitivity (determined in the laboratory) of 0.012 and $0.006 \mu\text{rad mbar}^{-1}$ for the north-south and east-west tilt-meters, respectively. The measurements are corrected for pressure variations using a microbarograph, having an accuracy of 5×10^{-2} mbar. The tilt data are filtered to remove frequencies higher than 1 Hz, and averaged at one point per minute. The east-west tiltmeter was affected by instrumental long-term drift and therefore is not used in the study.

Radon measurements. The radon probes are commercially available (as BARASOL). They consist of a cylindrical measurement chamber in equilibrium with the outside air through a diffusion filter. The decay of ²²²Rn is detected by a solid-state silicon detector. The counts are integrated over an hour. The sensitivity of the device is 50 Bq m^{-3} (1 count per hour). One autonomous probe was installed in the inner room in November 1995, and two other probes connected to a modem were added in the corridor in August 1996. One autonomous radon probe was also set in the soil at the Sur-Frètes ridge (Fig. 1) in November 1995.

Electrical measurements. We used second generation Pb/PbCl₂/kaolinite Petiau³⁰ unpolarizable electrodes. These electrodes are installed in 1.2 to 1.5 m deep, 40 cm diameter holes in 30 l of salted clay. This set-up was tested during an international comparison experiment³⁰, and was demonstrated to provide a stability of the order of 1 mV per year with a drift noise between 0.4 and 0.8 mV per month. The electric potential array is composed of 14 measurement points. The electrodes are combined into 20 dipoles in order to provide as much redundancy as possible. They are connected to a measuring station located on the ridge, through buried or aerial cables. The potential differences are recorded with a sampling rate of one per minute.

Correlation tests. The proportion of the rainfall, snowfall and snow-melting events which could be related to the radon bursts, assuming a maximal time delay of 10 d, amounts to 12% (out of 65 events; see Supplementary Information). For comparison, a similar value of 14% is obtained on average if the radon bursts are redistributed randomly. Therefore, no systematic relationship appears between these meteorological events and the radon bursts. Similarly, the transient electric potential variations are not systematically related to rainfall or snow melting. The proportion of these meteorological events which could be related to the transient electrical variations, assuming a maximal time delay of 10 d, amounts to 20% out of 42 events. For comparison, a similar value of 15% is obtained on average, if the electric signals are redistributed randomly.

Radon emanation in the laboratory. The equilibrium radon activity measurement performed on dry gneiss samples of $6 \times 10^{-5} \text{ m}^3$, using a measuring chamber having a free volume of $9 \times 10^{-4} \text{ m}^3$, amounts to 155 Bq m^{-3} . The radon emanation value of $8.3 \text{ atoms m}^{-2} \text{ s}^{-1}$ mentioned in the text was deduced without taking into account the internal porous surface of the sample.

Received 13 August 1998; accepted 4 March 1999.

1. Wakita, H., Nakamura, Y. & Sano, Y. Short-term and intermediate-term geochemical precursors. *Pure Appl. Geophys.* **126**, 267–278 (1988).
2. Igarashi, G. *et al.* Ground-water radon anomaly before the Kobe earthquake in Japan. *Science* **269**, 60–61 (1995).
3. Virk, H. S. & Singh, B. Radon recording of Uttarkashi earthquake. *Geophys. Res. Lett.* **21**, 737–740 (1994).
4. Raleigh, B. *et al.* The prediction of the Haicheng earthquake. *Eos* **58**, 236–272 (1977).
5. Corwin, R. F. & Morrison, H. F. Self-potential variations preceding earthquakes in Central California. *Geophys. Res. Lett.* **4**, 171–174 (1977).
6. Varotsos, P., Alexopoulos, K. & Lazaridou, M. Latest aspects of earthquake prediction in Greece by seismic electric signals, II. *Tectonophysics* **224**, 1–37 (1993).
7. Geller, R. J. (ed.) *Geophys. Res. Lett.* **23** (debate on “VAN” special issue) 1291–1452 (1996).
8. Pham, V. N., Boyer, D., Chouliaras, G., Le Mouél, J. L. & Rossignol, J. C. Characteristics of electromagnetic noise in the Ioannina region (Greece): a possible origin for so called “Seismic Electric Signal” (SES). *Geophys. Res. Lett.* **25**, 2229–2232 (1998).
9. Morrison, H. F., Fernandez, R. & Corwin, R. F. Earth resistivity, self potential variations, and earthquakes: a negative result for $M = 4.0$. *Geophys. Res. Lett.* **6**, 139–142 (1979).
10. Geller, R. J. Earthquake prediction: a critical review. *Geophys. J. Int.* **131**, 425–450 (1997).
11. Wyss, M. Second round of evaluations of proposed earthquake precursors. *Pure Appl. Geophys.* **149**, 3–16 (1997).

12. Scholz, C. H., Sykes, L. R. & Aggarwal, Y. P. Earthquake prediction: a physical basis. *Science* **181**, 803–810 (1973).
13. Igarashi, G., Wakita, H. & Sato, T. Precursory and coseismic anomalies in well water levels observed for the February 2, 1992 Tokyo Bay earthquake. *Geophys. Res. Lett.* **19**, 1583–1586 (1992).
14. Roeloffs, E. A. Hydrologic precursors to earthquakes: a review. *Pure Appl. Geophys.* **126**, 177–209 (1988).
15. Muir-Wood, R. & King, G. C. P. Hydrological signatures of earthquake strain. *J. Geophys. Res.* **98**, 22035–22068 (1993).
16. Mizutani, H., Ishido, T., Yokotura, T. & Onishi, S. Electrokinetic phenomena associated with earthquakes. *Geophys. Res. Lett.* **3**, 365–368 (1976).
17. Jouniaux, L. & Pozzi, J. P. Streaming potential and permeability of saturated sandstones under triaxial stress: consequences for electrotelluric anomalies prior to earthquakes. *J. Geophys. Res.* **100**, 10197–10209 (1995).
18. Bernard, P. Plausibility of long distance electrotelluric precursors to earthquakes. *J. Geophys. Res.* **97**, 17531–17546 (1992).
19. King, C. Y. Gas geochemistry applied to earthquake prediction: an overview. *J. Geophys. Res.* **91**, 12269–12281 (1986).
20. Morat, P. & Le Mouél, J. L. Electrical signals generated by the collapse of the pillars of a gypsum quarry. *C.R. Acad. Sci.* **308**, 33–38 (1989).
21. Perrier, F. et al. A one-year systematic study of electrodes for long period measurement of the electric field in geophysical environments. *J. Geomagn. Geoelectr.* **49**, 1677–1696 (1997).
22. Wilkening, M. H. & Watkins, D. E. Air exchange and ²²²Rn concentrations in the Carlsbad caverns. *Health Phys.* **31**, 139–145 (1976).
23. Direction de l'Équipement Électricité De France, Note de synthèse géologique et technique, *Barrage de Roselend, Fondation de l'Ouvrage 1–12*, (Électricité De France, Aix-en-Provence, 1952–1962). (In French.)
24. Roeloffs, E. A. Fault stability changes induced beneath a reservoir with cyclic variations in water level. *J. Geophys. Res.* **93**, 2107–2124 (1988).
25. Perrier, F., Trique, M., Hautot, S., Avouac, J. P. & Tarits, P. Electrical variations associated with yearly lake level variations. *Geophys. Res. Lett.* **25**, 1955–1958 (1998).
26. Simpson, D. W. & Negmatullaev, S. K. Induced seismicity at Nurek Reservoir, Tadjikistan, USSR. *Bull. Seismol. Soc. Am.* **71**, 1561–1586 (1981).
27. Gupta, H. K. Induced seismicity hazard mitigation through water level manipulation at Koyna, India: a suggestion. *Bull. Seismol. Soc. Am.* **73**, 679–682 (1983).
28. Silver, P. G. & Valette-Silver, N. J. Detection of hydrothermal precursors to large Northern California earthquakes. *Science* **257**, 1363–1367 (1992).
29. Rojstaczer, S., Wolf, S. & Michel, R. Permeability enhancement in the shallow crust as a cause of earthquake-induced hydrological processes. *Nature* **373**, 237–239 (1995).
30. Petiau, G. In *Proc. of the Workshop "Electrodes"* (eds Clerc, G., Perrier, F., Petiau, G. & Menvielle, M.) (Report, Centre de Recherches Géophysiques de Garchy, 1996).

Supplementary information is available on Nature's World-Wide Web site (<http://www.nature.com>) or as paper copy from the London editorial office of Nature.

Acknowledgements. We thank Y. Caristan, A. Meesters and R. Pican for support, and EDF for its water level data and access to the lakes. We also thank the members of the technical team from the Département Analyse et Surveillance de l'Environnement, CEA, for their dedication in performing their work in often difficult weather conditions.

Correspondence and requests for materials should be addressed to M.T. (e-mail: trique@ldg.bruiers.ceaf.fr).

Three-dimensional preservation of foot movements in Triassic theropod dinosaurs

Stephen M. Gatesy*, Kevin M. Middleton*, Farish A. Jenkins Jr† & Neil H. Shubin‡

* Department of Ecology and Evolutionary Biology, Brown University, Providence, Rhode Island 02912, USA

† Department of Organismic and Evolutionary Biology, and Museum of Comparative Zoology, Harvard University, Cambridge, Massachusetts 02138, USA

‡ Department of Biology, University of Pennsylvania, Philadelphia, Pennsylvania 19104, USA

Dinosaur footprints have been used extensively as biostratigraphic markers, environmental indicators, measures of faunal diversity and evidence of group behaviour^{1–5}. Trackways have also been used to estimate locomotor posture, gait and speed^{6–11}, but most prints, being shallow impressions of a foot's plantar surface, provide little evidence of the details of limb excursion. Here we describe Late Triassic trackways from East Greenland, made by theropods walking on substrates of different consistency and sinking to variable depths, that preserve three-dimensional records of foot movement. Triassic theropod prints share many features with those of ground-dwelling birds, but also demonstrate significant functional differences in position of the hallux (digit I), foot posture and hindlimb excursion.

Dinosaur trackways are common in the Ørsted Dal Member of

the uppermost Fleming Fjord Formation (Norian-Rhaetian) of Jameson Land, East Greenland¹². These strata consist of cyclically bedded fine-grained siliciclastic and carbonate-bearing units laid down as part of a large rift lake system¹³. Although the footprints are structurally diverse, almost all appear to be members of a gradational series (Fig. 1a–f). At one extreme are clearly preserved tridactyl tracks referable to the ichnogenus *Grallator* (*Anchisauripus*)^{1,14,15}. Such prints are commonly attributed to bipedal theropods¹⁶ and preserve impressions of digital pads, claws and, in some cases, skin (Fig. 1a). At the other extreme are tetradactyl, elongate prints in which the digital impressions are smooth channels constricting to narrow slits (Fig. 1f). The apparent impression of digit III is markedly longer than those of other digits; its distal end is elevated and expanded to resemble a fumarole-like crater. A posteromedially directed imprint of digit I is always present adjacent to an impression of the metatarsus. Most of the Ørsted Dal prints are intermediate in form between these two extremes (Fig. 1b–e).

The differences between tridactyl (Fig. 1a) and tetradactyl (Fig. 1f) tracks are comparable to those that have been used to distinguish faunal constituents and define ichnotaxa^{1,2}. However, two lines of evidence support the hypothesis that track variation is related to theropods traversing substrates of variable consistency, rather than to differences in foot morphology. First, some individual trackways exhibit more than one variant, although no single trackway preserves a complete gradational series. Second, guinea-fowl and turkeys walking on substrates of different consistencies closely duplicate the structural continuum of the Greenlandic prints (Fig. 1g–j). Whereas shallow prints on a relatively firm substrate accurately replicate the plantar form of these birds (Fig. 1g), successively deeper prints into increasingly wetter sediments record the entry of the initially splayed foot and the subsequent digital convergence as the foot is extracted (Figs 1h–j, 2a). Footprints in muds of intermediate consistency show separate entry and exit furrows for digits II and IV (Fig. 1h, i). In the deepest, wettest muds, the entire foot (with digits I–IV convergent) is extracted at the anterior end of the metatarsal-digit III furrow, raising a mound of sediment (Figs 1j, 2b). Thus, as mud hydration and penetration depth increase, bird tracks elongate because the substrate intercepts foot movements that normally occur above the surface. In the elongate Triassic footprints, the subsurface pathway of the toes disrupts sedimentary laminae, which can be seen in serial sections. These three-dimensional records confirm that, as in living birds, early Mesozoic theropods sank down and forward, and extracted the foot with convergent toes. Although evidence for slight digital approximation at the end of the stance phase has been reported from shallower tracks¹⁷, the elongate Greenlandic tracks document complete toe convergence, which is retained as a primitive feature among birds.

Although the general correspondence between extant avian and Greenlandic trackways reflects some pedal similarities, there are important functional differences between basal theropods and birds. The hallux (digit I) in ceratosaurs, such as *Coelophysus*, is sufficiently shorter than the other digits that on firm substrates it does not contact the ground (cf. Fig. 1a, b). The hallucal metatarsal, applied as a flattened splint to the midshaft of metatarsal II (Fig. 3), bears an asymmetrical condyle that permits a range of about 70° of flexion/extension and about 25° of ab/adduction of the metatarsophalangeal joint. The single interphalangeal joint, which is uniaxial, permits only flexion/extension. Fixation of metatarsal I and the configuration of the metatarsophalangeal and interphalangeal joints preclude retroversion. No known Late Triassic–Early Jurassic theropod shows evidence of an avian-like reversed hallux (*Eoraptor*, *Herrerasaurus*, *Coelophysus*, *Syntarsus*, *Procompsognathus*, *Segisaurus*, *Dilophosaurus*^{18–24}). Nonetheless, the posteromedially oriented hallucal print of some tracks, which appears superficially comparable to the impression of the posteriorly directed hallux of birds (compare